Journal of Electroanalytical Chemistry 713 (2014) 9–16

Contents lists available at ScienceDirect

Journal of Electroanalytical Chemistry

journal homepage: www.elsevier.com/locate/jelechem

Analysis of the hydrogen electrode reaction mechanism in thin-layer cells. 2. Study of hydrogen evolution on microelectrodes by scanning electrochemical microscopy

Horacio L. Bonazza, Leonardo D. Vega, José L. Fernández *

Programa de Electroquímica Aplicada e Ingeniería Electroquímica (PRELINE), Facultad de Ingeniería Química, Universidad Nacional del Litoral, Santiago del Estero 2829, S3000AOM Santa Fe, Santa Fe, Argentina

ARTICLE INFO

Article history:
Received 14 October 2013
Received in revised form 20 November 2013
Accepted 21 November 2013
Available online 1 December 2013

Keywords:
Hydrogen evolution reaction
Scanning electrochemical microscopy
Microelectrodes
Kinetic analysis
Thin layer cell

ABSTRACT

This work presents an updated equation for analyzing experimental dependences of the tip current (i_T) on the tip potential (E_T) and the tip-substrate distance (d) by scanning electrochemical microscopy (SECM). The model includes the contribution of a general thin layer cell (TLC) with no aprioristic restrictions about the reaction mechanism. The $i_T(E_T, d)$ dependence for a particular reaction is governed both by the microelectrode response (at large d values) and by the TLC response (more important at small d values) that result from solving the particular reaction mechanism. This equation was applied for studying the mechanism and for quantifying the elementary kinetic parameters of the hydrogen evolution reaction (*her*) on platinum and gold microelectrode tips. A dependence of the TLC current on E_T previously developed for the *her* operating through the Volmer–Heyrovsky–Tafel (VHT) mechanism was included in the model to correlate experimental $i_T(E_T, d)$ curves measured on these two metals. The transition from the VT to the VH route was clearly detected on both metals under conditions of high mass transport rates.

1. Introduction

The thin layer cell (TLC) is a valuable electrochemical configuration to carry out kinetic studies of electron-transfer reactions under steady state and high mass-transport rates. In addition to the well-known capacity of this setup for measuring rate constants of fast reactions [1–3], the TLC configuration is a rather powerful tool to reveal mechanistic details of electrocatalyzed multi-step reactions. The great simplicity of the steady-state mass-transport process in a TLC facilitates the rigorous mechanistic analysis of this type of reactions, as it was recently shown for the case of the hydrogen electrode reaction (HER) [4]. However, in spite of its straightforward theory, an ideal TLC experimental setup is not so easily obtained. Some problems such as alignment of the electrodes and ohmic drops across the electrode gap hampered the wide use of this electrochemical arrangement, regardless its apparently high potentiality for this type of study.

Probably the most widely available technique that allows the attainment of a TLC configuration is the scanning electrochemical microscope (SECM) [5]. This setup permits to build a TLC with variable and well-controlled separation between a microelectrode (usually a disk) and a flat microregion of a macroelectrode. Even though the SECM response convolutes a number of different mass-transport processes in addition to the TLC contribution, these processes are in general well modeled [6] and can be included in the theoretical formalism. The interaction between the TLC and the microelectrode responses constitutes the theoretical basis for the use of SECM for calculation of rate constants of single-step electrode reactions [7–9], which still is a developing issue [10,11]. On the basis of these developments and following the same strategies, it should be possible to generate a SECM formalism with an undefined general TLC contribution able to address the mechanism of each particular electrode reaction, independently of its complexity.

The HER has already been studied by SECM in different operation modes. On that sense, the hydrogen oxidation reaction on polycrystalline noble metals [12–14], multi-metallic catalysts [15] and supported nanoparticles [16–18] was mostly analyzed using feedback-based modes, although generation–collection modes were also employed [17–19]. On the other hand, the kinetics of hydrogen evolution reaction (*her*), either electrolytic or mediated by a redox reaction, was studied on Pt microelectrodes [12,20] and on ensembles of metal nanoparticles [17,21–23]. These works used approximate models to describe the *her* mechanism (rate determining step and quasiequilibrium-based formalisms [24]), and proved the usefulness of SECM to reveal mechanistic details of this reaction [23]. In a previous work [4], it was theoretically shown that the complete HER mechanism can be analyzed in a TLC setup through the *her*. This configuration can be experimentally attained with SECM in the feedback mode by setting the conditions that are shown in Scheme 1 [12]. In this case the

* Corresponding author. Tel.: +54 342 4571164x2519.
E-mail address: jlfernan@fiq.unl.edu.ar (J.L. Fernández).

1572-6657/$ - see front matter © 2013 Elsevier B.V. All rights reserved.
http://dx.doi.org/10.1016/j.jelechem.2013.11.027

her is analyzed on the tip microelectrode while the substrate (in this case Pt) functions under diffusion control as a regenerator of H^+ from tip-generated dissolved H_2. Thus, the tip potential (E_T) is varied over a cathodic range where H_2 evolution occurs, while the Pt substrate potential (E_S) is kept at a constant value where H_2 is oxidized back to H^+ under diffusion control. The steady-state dependence of the tip current (i_T) on E_T is then recorded and analyzed at different tip-substrate distances (d). This setup was already used by Bard and co-workers to measure the apparent rate constant and transfer coefficient of the *her* on Pt tips [12] by processing the results using the classical theory previously developed for a quasi-reversible one-step reaction [8]. Nevertheless, by incorporating the recently reported TLC formalism of the *her* [4] in the SECM theoretical equations, it should also be possible to carry out a mechanistic analysis of this reaction and the quantification of the complete set of elementary rate constants. In this context, this work reports a general equation to interpret $i_T(E_T, d)$ dependences, which incorporates the TLC contribution in such a way that any reaction mechanism can be accounted. This model was used to analyze the *her* mechanism on two metals that represent limiting performances, as are Pt (highly active) and Au (poorly active).

2. Materials and methods

2.1. Chemicals and materials

All electrochemical experiments were carried out in 0.02 M $HClO_4$ (Merck) with 0.1 M $LiClO_4$ as supporting electrolyte. Water was first deionized with an exchange resin, then doubly distilled, and finally treated with a Purelab purifier (Elga Labwater, resistivity $\geqslant$18.2 MΩ cm). High purity (>99.999%) Pt and Au wires and foils (Goodfellow) were employed.

2.2. Tip fabrication

Pt and Au tips were fabricated by heat sealing of sharpened wires into borosilicate glass capillaries following a procedure previously described [25]. Briefly, pieces of 25-μm-diameter Pt and Au wires (Goodfellow) were soldered to copper wires using a micropoint soldering machine (S&H Dental, Argentina), and electrochemically sharpened at the end. Sharpening of Pt wires was carried out by application of an AC voltage (sine wave, 50 Hz, ±2.5 V peak to peak) against a concentric annular Pt counter-electrode (5 mm opening) in 4.5 M $CaCl_2$ – 1 M HCl. Sharpening of Au wires was carried out similarly, but using a Au counter-electrode and applying a DC voltage (2 V) in 1 M HCl. The sharpened wires were then introduced into borosilicate glass capillaries (1 mm outer diameter, 0.1 mm thickness), which ends were melted by careful heating under a torch flame until the sealing of about 2 mm of the etched wires was visually verified. Heating was continued until the exposition of a protruding metal tip totally or partially covered by a thin glass layer was verified. The capillaries were embedded into cylindrical acrylic supports and polished until the exposure of the metal disk surrounded by a complete glass ring was verified. Then the acrylic supports were removed by dissolution in chloroform and the tips were ultrasonically cleaned in acetone and finally rinsed with water. The tip dimensions were estimated by cyclic voltammetry and SECM approach curves in 0.001 M ferrocene methanol solution, in addition to observation by optical microscopy (Nikon Optiphot with a FX-35DX camera).

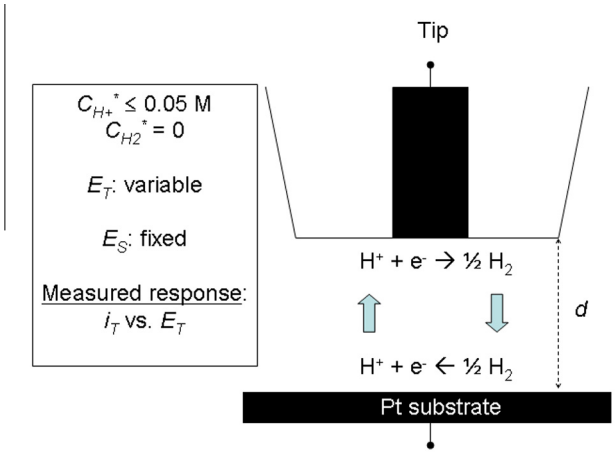

Scheme 1. Conditions for studying the *her* on tip microelectrodes by SECM.

2.3. SECM experiments

A home-built SECM instrument with typical components [26] (bipotentiostat and micropositioning system) was used. The bipotentiostat was a PG 340 (Heka Elektronik, Germany) with an ITC-16 board. The tip position was controlled with three stepper motors (Zaber, Canada) and a Nanocube P-611.3S closed-loop XYZ nanopositioning system driven by an E-664 voltage amplifier/servo controller (Physik Instrumente, Germany). Both the bipotentiostat and the positioning system were commanded via the software PotMaster (Heka Elektronik). The Teflon cell had a typical configuration, with a Pt foil functioning as the substrate and a gold wire counter-electrode. The reference electrode was a saturated calomel electrode (SCE), but all potentials were reported respect to the reversible hydrogen electrode (RHE).

The tips were approached to the substrate using the H^+/H_2 couple as mediator under total positive feedback [12,13]. A cathodic potential was applied to the tip such as the proton reduction reaction operated under proton-diffusion control. As it is observed in the tip cyclic voltammograms shown in Fig. 1, the range of potentials to reach this condition was different for each metal, since it depends on the activity of each material for this reaction. Thus, the approach potential for Pt tips was −0.6 V vs. RHE, while for Au tips it was −1.2 V vs. RHE. Besides, the Pt-substrate potential was kept at 0.5 V vs. RHE to operate the oxidation of the tip-generated H_2 under diffusion control. In the case of Au tips, the approach was stopped as soon as the current verified a slight increase (typically 10% of its infinite-distance value). From this point, the

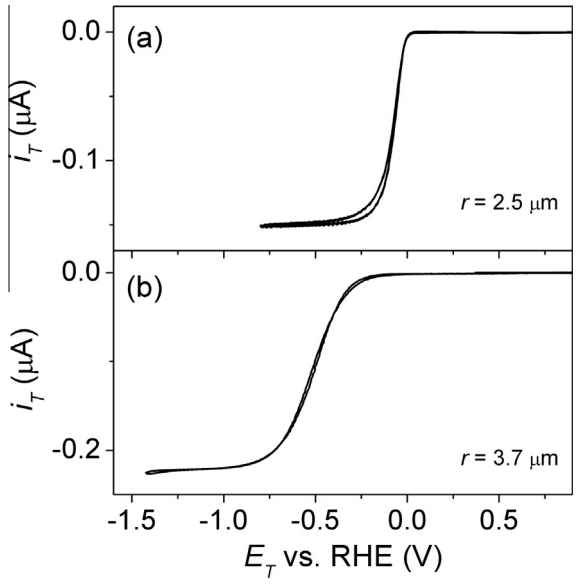

Fig. 1. Cyclic voltammograms of Pt (a) and Au (b) tips in 0.02 M $HClO_4$ – 0.1 M $LiClO_4$. $v = 0.1$ V s^{-1}.

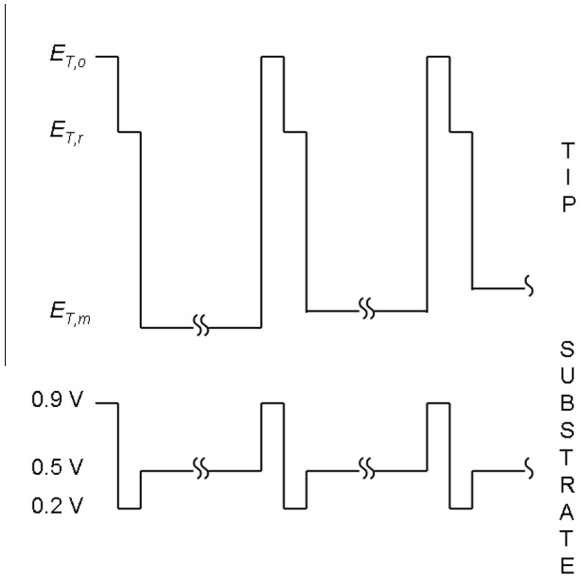

	$E_{T,o}$ (V)	$E_{T,r}$ (V)	$E_{T,m}$ (V)
Pt	1.3	0.2	-0.9 – 0.2
Au	1.8	0.2	-1.2 – 0.2

Scheme 2. Potential-step sequences applied to the tip and the substrate for measurement of steady-state $i_T(E_T)$ SECM curves for the *her*. The step potential values (vs. RHE) used for the Pt and Au tips are indicated in the inserted table.

tips were slowly approached until the desired current increase was reached, thus avoiding their physical contact with the Pt substrate. This was particularly critical to prevent contamination of Au tips with Pt.

Steady-state measurements of the *her* were carried out point by point by applying the program of potential-step sequences that is shown in Scheme 2. Each step sequence applied to the tip included an oxidation potential ($E_{T,ox}$, 5 ms) for cleaning the tip surface, a reduction potential ($E_{T,red}$, 5 ms) for reduction of formed oxides, and a measuring potential ($E_{T,m}$, 20 s) that varied over the analyzed potential range in intervals of 0.025 V. These values were different on Pt and Au, and are indicated in Scheme 2. Simultaneously, the substrate potential was also controlled during the cleaning, reduction, and measuring steps. The cleaning (or oxidation) potential applied to the substrate was sufficiently low to avoid dissolution of Pt traces. The tip current was registered during application of the measuring potential, and the attainment of the steady state was verified by its constancy in time. The mean current at each tip potential was measured by averaging the current values registered during the last half of the measuring periods.

3. Theory

3.1. General model

The model that incorporates the TLC contribution into the dependency of the SECM tip current on E_T and on the normalized tip-substrate distance ($L = d/a$, where d is the tip-substrate distance and a is the disk radius) was initially developed by Mirkin et al. [8], and widely used for quasi-reversible single-step reactions [6,27–33]. On the basis of this model, the analytical expression for the normalized tip current (I_T) given by Eq. (1) is proposed here. This equation includes the parallel inputs of the TLC process (I_{TLC}) and of the reaction at the disk microelectrode (I_{disk}), given by Eqs. (2) and (3), respectively.

$$I_T(E_T, L) = I_{TLC}(E_T, L) + I_{disk}(E_T, L) \tag{1}$$

$$I_{TLC}(E_T, L) = \left(\frac{i_{TLC}(E_T, L)}{i_{T,\infty}}\right)\left(\frac{I_{PF}(L) - I_{NF}(L)}{\frac{\pi}{4L\beta(R_g)}}\right) \tag{2}$$

$$I_{disk}(E_T, L) = \left(\frac{i_{disk}(E_T)}{i_{T,\infty}}\right) I_T^{NF}(L) \tag{3}$$

The I_T value is normalized respect to the diffusion-controlled tip current at infinite distance ($I_T = i_T/i_{T,\infty}$, where $i_{T,\infty} = 4\beta nFDCa$), where n is the number of exchanged electrons, F is the Faraday constant, D and C are the diffusion coefficient and bulk concentration of the reacting species. Besides, the term β takes into account the effect of the R_g both on the SECM approach curves and on $i_{T,\infty}$ [6]. The TLC contribution given by Eq. (2) involves the intrinsic TLC current density since $i_{TLC}/i_{T,\infty} = j_{TLC}/j_{T,\infty}$, where $j_{T,\infty} = i_{T,\infty}/\pi a^2$. This normalized TLC current is affected by a term that guarantees the accomplishment of the tip current limiting behaviors, which are defined by the negative (I_{NF}) and positive (I_{PF}) feedback currents. On the other hand, the contribution of the disk microelectrode current given by Eq. (3) involves the normalized disk current at infinite distance ($i_{disk}/i_{T,\infty}$), which also depends on the reaction kinetics, affected by the blocking effect of the substrate. This blocking effect can be properly accounted by the negative feedback current.

3.2. Quasi-reversible reaction

The core of Eq. (1) is the TLC current, which dependence on the tip potential and on the tip-substrate distance is governed by the kinetics and mechanism of the analyzed reaction. Differently to the previous approach where the TLC contribution was specifically introduced for a quasi-reversible reaction [8], this equation leaves undefined the $I_{TLC}(E_T,L)$ dependence, thus expanding its applicability. Thus for example, for the quasi-reversible reduction of O to R, the introduction of the $I_{TLC}(E_T,L)$ and the $I_{disk}(E_T,L)$ dependences for a Buttler–Volmer reaction [34,35], leads to the complete $I_T(E_T,L)$ dependence given by Eq. (4), where $\Lambda = k^o a/D_O$ (k^o is the standard rate constant), α is the symmetry factor, $\gamma = D_O/D_R$, $\Theta = \exp[f(E_T - E^{ref})]$, and $E^{ref} = E^{o\prime}$ (formal potential of the reaction).

$$I_T(E_T, L) = \frac{I_{PF}(L) - I_{NF}(L)}{1 + \gamma\Theta + \frac{\Theta^{\alpha}}{\Lambda L}} + \frac{I_{NF}(L)/\beta(R_g)}{1 + \gamma\Theta + \frac{4\Theta^{\alpha}}{\Lambda}\left[\frac{8(1+\gamma\Theta)+3\Theta^{\alpha}/\Lambda}{16(1+\gamma\Theta)+3\pi\Theta^{\alpha}/\Lambda}\right]} \tag{4}$$

This equation is similar to that originally developed by Mirkin et al. (Eq. 25 in Ref. [8]). However, as Eq. (4) can be used together with any of the R_g-dependant functions reported up today for I_{PF} and I_{NF} [6], its application is extended to tips with any R_g value.

3.3. The hydrogen evolution reaction

The dependence of the TLC current density for the *her* operating through the Volmer–Heyrovsky–Tafel mechanism was already developed in Ref. [4]. This equation takes into account the functionality of the coverage of $H_{(ad)}$ (θ) on the potential assuming a Langmuir-type isotherm. The involved kinetic parameters are the rates of the elementary steps (v_i^e) and the coverage of $H_{(ad)}$ (θ^e) evaluated at the equilibrium potential for the same bulk concentration of H^+ (C^*_{H+}) and hydrogen pressure (P_{H2}) of 1 atm. It is quite straightforward to modify this equation to take into account a more complex description of the adsorption, for example by introduction of the Frumkin interaction parameters u through the term $\Gamma = e^{u(\theta-\theta e)}$ and of the symmetry factor of the adsorption reaction (λ) [36]. By including these terms in the reported equation for the *her* TLC current density, reordering and normalizing it respect to $j_{T,\infty}$, it is possible to obtain the dependence of the normalized

TLC tip current for the *her* ($j^{her}_{TLC}/j_{T,\infty} = i^{her}_{TLC}/i_{T,\infty}$) on E_T and L that is shown in Eq. (5).

$$\frac{i^{her}_{TLC}(E_T,L)}{i_{T,\infty}} = \frac{\left(\frac{\pi}{4\beta L}\right)\left\{V^e_V\left[\left(\frac{1-\theta}{1-\theta^e}\right)\Theta^{-1} - \left(\frac{\theta}{\theta^e}\right)\Gamma\right]\Theta^{\alpha} + V^e_H\left(\frac{\theta}{\theta^e}\right)\Gamma\Theta^{-(1-\alpha)}\right\}}{\frac{\Gamma^{\lambda}}{L} + \left\{V^e_V\left(\frac{1-\theta}{1-\theta^e}\right)\Theta^{-1} + V^e_H\left[\left(\frac{\theta}{\theta^e}\right)\Gamma\Theta^{-1} - \xi\left(\frac{1-\theta}{1-\theta^e}\right)\right]\right\}\Theta^{\alpha}}$$
$$= \frac{\left(\frac{\pi}{4\beta L}\right)\left\{V^e_V\left[\left(\frac{1-\theta}{1-\theta^e}\right)\Theta^{-1} - \left(\frac{\theta}{\theta^e}\right)\Gamma\right]\Theta^{\alpha} - V^e_T\left(\frac{\theta}{\theta^e}\right)^2\Gamma^{(2-\lambda)}\right\}}{\frac{\Gamma^{\lambda}}{2L} + \left[V^e_V\left(\frac{1-\theta}{1-\theta^e}\right)\Theta^{-(1-\alpha)} - V^e_T\xi\left(\frac{1-\theta}{1-\theta^e}\right)^2\Gamma^{-\lambda}\right]}$$
$$= \frac{\left(\frac{\pi}{4\beta L}\right)\left(\frac{\theta}{\theta^e}\right)\Gamma\left[V^e_H\Theta^{-(1-\alpha)} + V^e_T\left(\frac{\theta}{\theta^e}\right)\Gamma^{(1-\lambda)}\right]}{\frac{\Gamma^{\lambda}}{2L} + \left\{V^e_H\left[\left(\frac{\theta}{\theta^e}\right)\Gamma\Theta^{-1} + \xi\left(\frac{1-\theta}{1-\theta^e}\right)\right]\Theta^{\alpha} + V^e_T\xi\left(\frac{1-\theta}{1-\theta^e}\right)^2\Gamma^{-\lambda}\right\}} \tag{5}$$

This equation includes the equilibrium rates of the elementary steps normalized according to the relationship $V^e_i = \upsilon^e_i a/(D_{H+}C^*_{H+}$ (where i: V, H, T). Besides, in this case E^{ref} involved in Θ is the potential of the hydrogen reference electrode at C^*_{H+} and P_{H2} = 1 atm. Then, the parameter ξ groups the diffusion coefficients and bulk concentrations of H^+ and dissolved H_2 according to $\xi = D_{H+}C^*_{H+}/(2D_{H2}C^*_{H2+})$ [4], which in this case results $\xi = C^*_{H+}/3.59\times10^{-4}(\mathrm{dm^3\,mol^{-1}})$ [37]. Note that the θ (E_T) dependency is defined in Eq. (5) and can be obtained for example by reordering the last identity in this equation.

The second kinetically effected term that is involved in Eq. (1) for the *her* is the response of the disk microelectrode tip, that is $i^{her}_{disk}(E_T)/i_{T,\infty}$. This functionality corresponds to the polarization curve of a disk microelectrode for the *her*, whose general expression (valid for any pH) was recently obtained under the assumption of uniform accessibility [37]. In fact, as in SECM experiments the H^+ concentration varies over a restricted interval (typically $0.005\,\mathrm{M} < C^*_{H+} < 0.06\,\mathrm{M}$ [12]) and the bulk concentration of dissolved H_2 is null ($C^*_{H2} = 0$), the resulting dependence (relative to $i_{T,\infty}$) of the *her* on a disk tip can be simplified into Eq. (6). This equation is valid as long as the potential for water discharge [37] is not reached.

$$\frac{i^{her}_{disk}(E_T)}{i_{T,\infty}} = \frac{V^e_V\left[\left(\frac{1-\theta'}{1-\theta^e}\right)\Theta^{-1} - \left(\frac{\theta'}{\theta^e}\right)\Gamma\right]\Theta^{\alpha} + V^e_H\left(\frac{\theta'}{\theta^e}\right)\Gamma\Theta^{-(1-\alpha)}}{\left(\frac{4\beta}{\pi}\right)\Gamma^{\lambda} + \left\{V^e_V\left(\frac{1-\theta'}{1-\theta^e}\right)\Theta^{-1} + V^e_H\left[\left(\frac{\theta'}{\theta^e}\right)\Gamma\Theta^{-1} - \xi\left(\frac{1-\theta'}{1-\theta^e}\right)\right]\right\}\Theta^{\alpha}}$$
$$= \frac{V^e_V\left[\left(\frac{1-\theta'}{1-\theta^e}\right)\Theta^{-1} - \left(\frac{\theta'}{\theta^e}\right)\Gamma\right]\Theta^{\alpha} - V^e_T\left(\frac{\theta'}{\theta^e}\right)^2\Gamma^{(2-\lambda)}}{\left(\frac{2\beta}{\pi}\right)\Gamma^{\lambda} + V^e_V\left(\frac{1-\theta'}{1-\theta^e}\right)\Theta^{-(1-\alpha)} - V^e_T\xi\left(\frac{1-\theta'}{1-\theta^e}\right)^2\Gamma^{-\lambda}}$$
$$= \frac{\left(\frac{\theta'}{\theta^e}\right)\Gamma\left[V^e_H\Theta^{-(1-\alpha)} + V^e_T\left(\frac{\theta'}{\theta^e}\right)\Gamma^{(1-\lambda)}\right]}{\left(\frac{2\beta}{\pi}\right)\Gamma^{\lambda} + V^e_H\left[\left(\frac{\theta'}{\theta^e}\right)\Gamma\Theta^{-1} + \xi\left(\frac{1-\theta'}{1-\theta^e}\right)\right]\Theta^{\alpha} + V^e_T\xi\left(\frac{1-\theta'}{1-\theta^e}\right)^2\Gamma^{-\lambda}} \tag{6}$$

It should be noted that as Eq. (6) was obtained under the uniform accessibility assumption, it is similar to the TLC current with an electrode distance equal to the diffusion layer thickness (δ), that in this case is $\delta = \pi a/4\beta$. In this equation, θ' represents the $H_{(ad)}$ coverage that should be verified on the tip at infinite distance for a set of kinetic parameters. Similarly to θ, its dependency on E_T can be obtained from the second or third identity in Eq. (6).

The application of Eq. (1) for studying the *her* can be completed by assuming the functionality of I_{NF} and I_{PF} on L and R_g, by instance given by Eqs. (7) and (8) [6]. The parameters α' (R_g) and $\beta(R_g)$, defined by Eqs. (9) and (10) respectively [6,38], permit to take into account the effect of the tip R_g on the positive and negative feedback currents.

$$I_{NF}(L) = \frac{\frac{2.08}{R_g^{0.358}}\left(L - \frac{0.145}{R_g}\right) + 1.585}{\frac{2.08}{R_g^{0.358}}(L + 0.0023R_g) + 1.57 + \frac{\ln(R_g)}{L} + \frac{2}{\pi R_g}\ln\left(1 + \frac{\pi R_g}{2L}\right)} \tag{7}$$

$$I_{PF}(L) = \alpha'(R_g) + \frac{\pi}{4\beta(R_g)\mathrm{ArcTan}L} + \frac{2}{\pi}\left(1 - \alpha'(R_g) - \frac{1}{2\beta(R_g)}\right)\mathrm{ArcTan}L \tag{8}$$

$$\alpha'(R_g) = \ln 2 + \ln 2\left(1 - \frac{2}{\pi}\mathrm{ArcCos}\frac{1}{R_g}\right) - \ln 2\left[1 - \left(\frac{2}{\pi}\mathrm{ArcCos}\frac{1}{R_g}\right)^2\right] \tag{9}$$

$$\beta(R_g) = 1 + 0.639\left(1 - \frac{2}{\pi}\mathrm{ArcCos}\frac{1}{R_g}\right) - 0.168\left[1 - \left(\frac{2}{\pi}\mathrm{ArcCos}\frac{1}{R_g}\right)^2\right] \tag{10}$$

4. Results and discussion

4.1. Descriptive capability

The behavior of the TLC current density for the Volmer–Heyrovsky–Tafel mechanism was already fully analyzed previously [4]. With the goal to visualize the manifestation of these features in the SECM response, some $I_T(E_T,L)$ curves were calculated with Eqs. (1)–(3) and (5)–(10) using the software Mathcad (version 2000). Different kinetic parameters that are representative of typical electrode behaviors were selected in these calculations. Thus for example, the curves shown in Fig. 2 provide a concrete view of the effect that should be expected when approaching the tip to the substrate for two different mechanistic situations. On the one hand, Fig. 2-I shows situations where the equilibrium rates are very large, so that the *her* response on an disk microelectrode approaches to the diffusion-controlled (reversible) behavior. It is possible to see that in this type of situation the polarization curves are poorly sensitive to variations in υ^e_V over more than two orders of magnitude. Thus, in this case the *her* curves measured on a disk microelectrode are hardly useful to make a precise estimation of this parameter over this range of values. However, as the tip is approached to the substrate, for example to a distance L = 0.1, the contribution of the TLC added to the *her* polarization curve becomes more important and the mass transport rate is significantly increased. Under these conditions the curves calculated for different values of υ^e_V are clearly distinguished, even for the largest υ^e_V values. Thus, the use of $I_T(E_T)$ dependences obtained at small L values is particularly suitable for accurate calculation of the kinetic parameters of fast elementary rates of the *her*. On the other hand, a similar situation is shown in Fig. 2-II, which emphasizes the effect of the ratio of the Tafel and Heyrovsky rates. While the response of the isolated disk is barely influenced by the mechanistic features, the SECM $I_T(E_T)$ dependence for a small L value is clearly affected by the transition between routes (evidenced by a shoulder), which in this case is strongly dependent on the value of υ^e_T.

Moreover, the curves in Fig. 3 show the effect of the tip-substrate distance, both in conditions where the equilibrium rates are very large (Fig. 3-I) and where the transition between routes should occur (Fig. 3-II). These plots highlight that the use of these curves to analyze the *her* on a highly active material is benefited when the tip is approached to a distance $L \leqslant 0.4$, which implies at least a three-fold increase in the value of i_T respect to $i_{T,\infty}$. Only under these conditions the mechanistic features can be detected and analyzed from the $I_T(E_T)$ curves with the purpose to obtain the complete set of kinetic parameters on a highly active material.

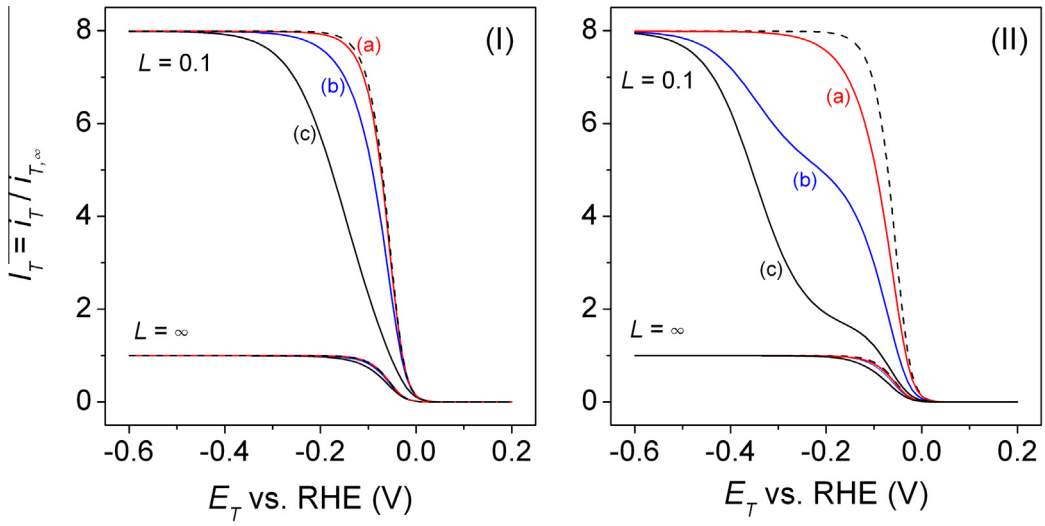

Fig. 2. SECM $I_T(E_T)$ dependences for the *her* calculated with Eqs. (1)–(3) using different kinetic parameters for $L = 0.1$ and ∞. $R_g = 5$. $C^*_{H+} = 0.02$ M. Kinetic parameters: $\theta^e = 0.2$, $u(RT) = 0.3$, $\alpha = \lambda = 0.5$. $V^e_i = v^e_i a/(D_{H+}C^*_{H+})$: (I) $V^e_V = 100$ (a), 10 (b), 1 (c), $v^e_H = 0.01$, $V^e_T = 10$. (II) $V^e_V = 10$, $v^e_H = 0.001$, $V^e_T = 1$ (a), 0.1 (b), 0.03 (c). Dashed lines are the diffusion-controlled dependences.

The contribution of each of the two terms involved in Eq. (1) can be better analyzed in the graphs presented in Fig. 4. These curves show the TLC and disk currents (in addition to the tip current) calculated under total diffusion control with Eqs. (2) and (3) as a function of L. For L values smaller than 0.5, the TLC response conforms more than 80% of the total tip current (as is better observed in Fig. 4b), while the disk current becomes the predominant contribution for $L > 2$.

It should be remarked that the main advantage of using this SECM-based configuration to study the *her* on microelectrodes is the inclusion of a well-controlled variable (the tip-substrate distance) that affects the mass-transport rate, in addition to the microelectrode size. Thus for example, an increase of one order of magnitude of the limiting current density for the *her* that is verified on a microelectrode can be reached either by decreasing the disk radius that magnitude (i.e. from 10 to 1 μm) or by approaching the tip to a tip-substrate distance of about one tenth of the radius ($L \cong 0.08$).

4.2. SECM study of the her on Pt tips

The *her* was studied in this work by SECM $I_T(E_T, L)$ curves on Pt tips pursuing two objectives. On one hand, this analysis permits to visualize the capability of the equations to correlate experimental curves obtained on a well-known electrocatalyst for the *her*, as it is Pt. On the other hand, this model system is adequate to evaluate the sensitivity of the correlations to the involved adjusted kinetic parameters.

In fact, the *her* was already studied on Pt through the fitting of SECM $I_T(E_T,L)$ curves by Bard and co-workers [12]. That study was carried out on a 25-μm-diameter Pt tip ($C^*_{H+} = 0.01$ M; $i_{T,\infty} = -311.3$ nA), and the reaction was interpreted under the assumption of a quasi-reversible model. Thus, the values of k^o and α were estimated using the classical theory [8]. In order to carry out a deeper mechanistic analysis, Eqs. (1)–(3) were used to fit these earlier results and to estimate the full set of elementary kinetic parameters that consistently reproduces these published

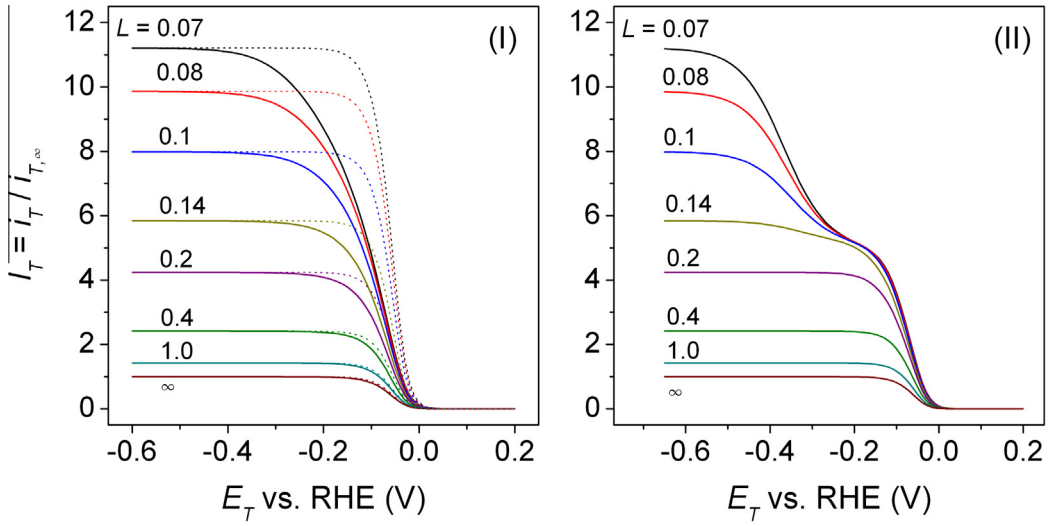

Fig. 3. SECM $I_T(E_T)$ dependences for the *her* calculated with Eqs. (1)–(3) using different values of L (indicated in the graphs). $R_g = 5$. $C^*_{H+} = 0.02$ M. Kinetic parameters: $\theta^e = 0.2$, $u(RT) = 0.3$, $\alpha = \lambda = 0.5$. $V^e_i = v^e_i a/(D_{H+}C^*_{H+})$: (I) $V^e_V = 10$, $v^e_H = 0.01$, $V^e_T = 0.2$. (II) $V^e_V = 100$, $v^e_H = 0.001$, $V^e_T = 0.1$. Dashed lines are the diffusion-controlled dependences.

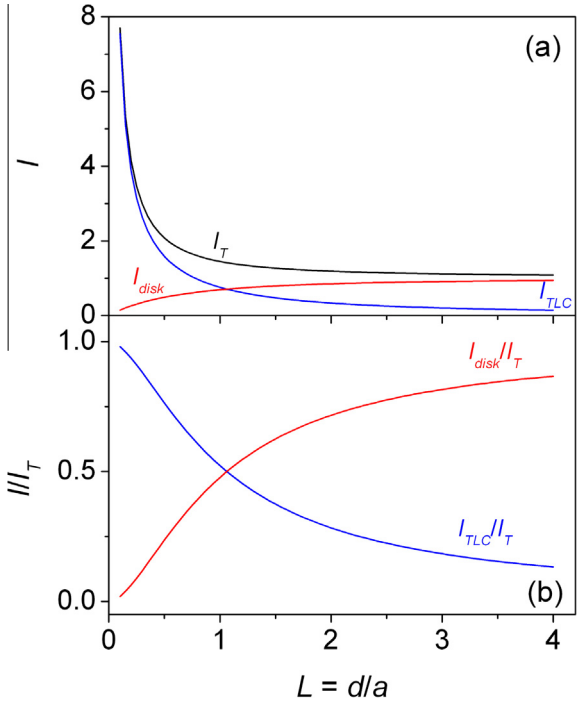

Fig. 4. Dependences on L of the TLC (I_{TLC}) and disk microelectrode (I_{disk}) contributions to the normalized tip current (I_T) for the *her* (a), and the same dependences relative to I_T (b). $E_T = -0.5$ V vs. RHE; $R_g = 5$. $C^*_{H+} = 0.02$ M. Kinetic parameters: $V^e_V = 10$, $v^e_H = 0.0001$, $V^e_T = 0.5$, $\theta^e = 0.2$, u(RT) = 0.3, $\alpha = \lambda = 0.5$.

curves. The equilibrium rates and coverage were freely varied in these fittings, while the other kinetic parameters (u, α and λ) were kept invariant in their accepted values for Pt. The resulting correlations that are shown in Fig. 5 indicate that the *her* follows the Volmer–Tafel route at low potentials, which led to the parameters shown in Table 1 (first row). Besides, no evidence of a route transition is detected in this data, as probably the mass-transport rates required to observe this process (affected both by the tip size and distance) were not reached.

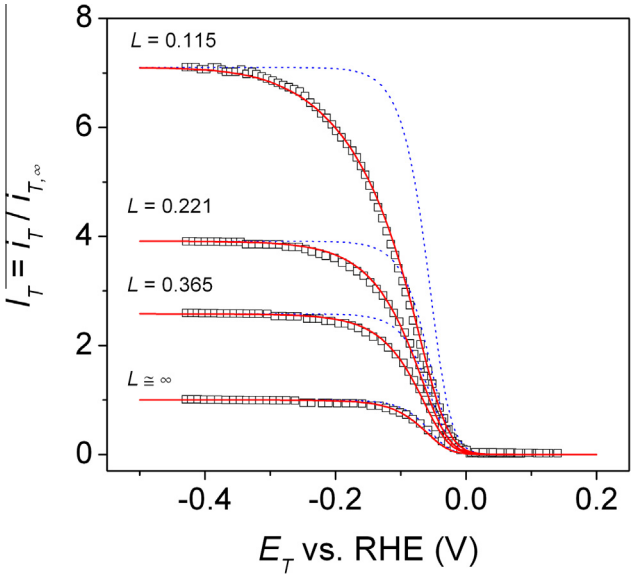

Fig. 5. Correlations with Eqs. (1)–(3) (solid lines) of reported SECM $I_T(E_T,L)$ dependences for the *her* [12] on a Pt tip (symbols). $C^*_{H+} = 0.01$ M. $a = 12.5$ μm; $R_g = 11$; $i_{T,\infty} = -311.3$ nA. Dashed lines are the diffusion-controlled dependences.

Furthermore, SECM $I_T(E_T,L)$ curves for the *her* were measured in this work on a 2.5-μm-radius Pt tip ($R_g \cong 2.3$) in perchloric acid solution ($C^*_{H+} = 0.02$ M; $i_{T,\infty} = -149.5$ nA) and correlated with Eqs. (1)–(3). These experimental curves, as well as the resulting correlations that were reached with a unique set of kinetic parameters (presented in Table 1, second row) for all curves, are shown in Fig. 6. These parameters are in the order of those reported for Pt in these pH conditions [37], and indicates that the *her* proceeds through the Volmer–Heyrovsky route at high overpotentials. Such a behavior was also detected by SECM on ensembles of Pd nanoparticles [23]. It is important to remark that while the correlations of curves measured at $L > 0.2$ are poorly sensitive to some of the kinetic parameters shown in Table 1 (i.e. to v^e_H), the curves measured at $L < 0.2$ show features that can only be reproduced with this particular set. This occurs because the transition from the Volmer–Tafel to the Volmer–Heyrovsky route is effective only at potentials $E_T < -0.4$ V vs. RHE, where the reaction already reached the mass-transport limitation for the larger L values. These values are in accordance with the parameters determined from the results measured by Bard et al. [12] excepting for the Tafel elementary rate, which is more than one order of magnitude larger in this work. This is not surprising, since the curves shown in Fig. 6 were obtained on a pre-activated electrode, which was cleaned by an anodic pulse just before the acquisition of each point of the curve.

The results obtained from the application of the developed SECM theoretical formalism to study the *her* on Pt, both on our own measurements and on reported data, validate the presented SECM methodology. Thus, this procedure can be applied for studying the *her* on other electrode materials with a high degree of confidence.

4.3. SECM study of the her on Au tips

SECM $I_T(E_T, L)$ curves for the *her* measured on a 3.7-μm-radius Au tip ($R_g \cong 3$) in perchloric acid solution ($C^*_{H+} = 0.02$ M; $i_{T,\infty} = -218.5$ nA) are shown in Fig. 7. As it was already observed in the cyclic voltammogram presented in Fig. 1b, the *her* requires much larger overpotentials on gold than on platinum to reach diffusion limiting conditions [13]. The steady-state $I_T(E_T)$ curve measured on the isolated tip shows typical features of an irreversible reaction. However, as soon as the tip approaches the substrate surface and the TLC contribution becomes perceptible, a shift of the whole polarization curve toward slightly larger currents is observed. Upon continuing approaching the tip to the substrate, the tip limiting currents keep increasing as expected, but the currents at the lower overpotentials remain almost at similar values (almost independent of L). Globally, what can be observed from these curves is that the $I_T(E_T)$ dependences evolve from essentially a typical irreversible behavior at infinite distance to a response full of mechanistic features at decently small distances ($L < 0.6$). Moreover, the correlations of these experimental curves with Eqs. (1)–(3), represented with solid lines in Fig. 7, led to the kinetic parameters that are shown in Table 1 (third row). Remarkably, all curves can be correlated with parameters whose values are quite similar. These values, particularly v^e_T and θ^e, are in agreement with those previously reported for this metal in very acid condition [39]. The most significant aspects about these calculated parameters are the very low values of v^e_V and of θ^e (which implies a large equilibrium constant for desorption of adsorbed hydrogen, or the Tafel step [37]). These two magnitudes, together with the very small values of the Heyrovsky elementary rate constant, cause the significantly low electrocatalytic activity of this metal for the *her*. As on Pt, the *her* proceeds on Au through the Volmer–Tafel route at the less cathodic potentials (typically down to $E_T \cong -0.7$ V vs. RHE), and from this potential to more cathodic values the Volmer–Heyrovsky route becomes predominant.

Table 1
Kinetic parameters resulting from correlations of SECM $I_T(E_T,L)$ curves for the *her*. v_i^e in mol s^{-1} cm^{-2}, u (in RT units) = 0.3, $\alpha = \lambda = 0.5$.

Metal	C^*_{H+} (mol dm^{-3})	v^e_V	v^e_H	v^e_T	θ^e	Source
Pt	0.01	4.4×10^{-6}	$<1 \times 10^{-9}$	6.8×10^{-8}	0.21	[12]
Pt	0.02	1.8×10^{-5}	6.3×10^{-10}	1.47×10^{-6}	0.20	This work
Au	0.02	5.5×10^{-10}	7.3×10^{-15}	5.9×10^{-9}	0.05	This work

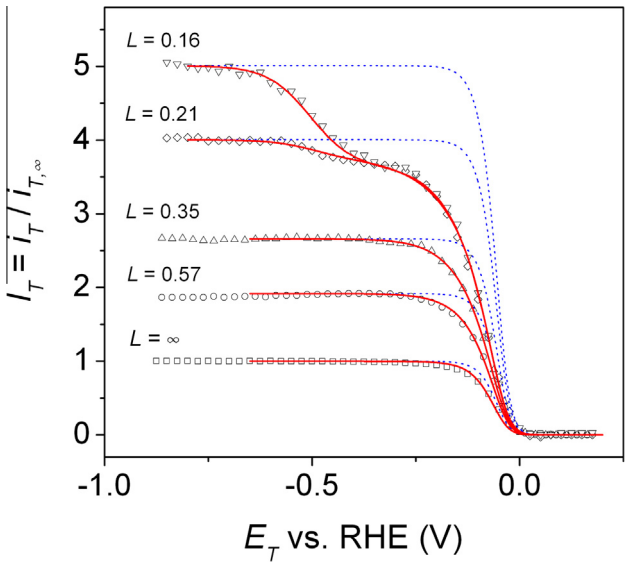

Fig. 6. Experimental SECM $I_T(E_T,L)$ dependences for the *her* measured on a Pt tip (a = 2.5 μm; R_g = 2.3; $i_{T,\infty}$ = −149.5 nA) in 0.02 M $HClO_4$ – 0.1 M $LiClO_4$ (symbols), and correlations of these curves performed with Eqs. (1)–(3) (solid lines). Dashed lines are the diffusion-controlled dependences.

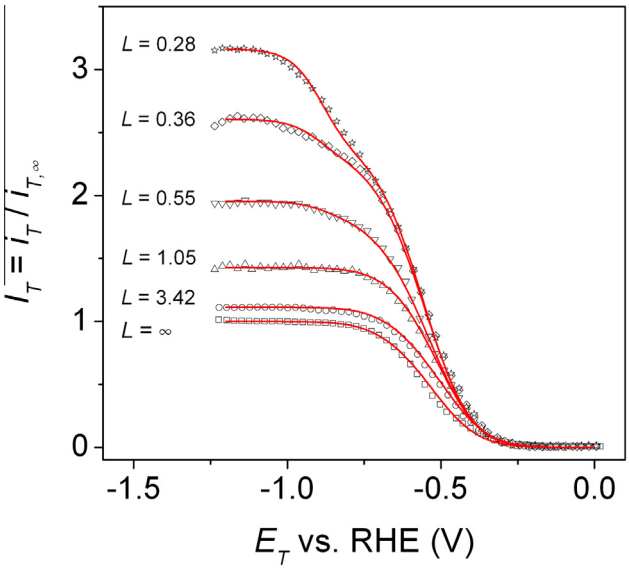

Fig. 7. Experimental SECM $I_T(E_T,L)$ dependences for the *her* measured on a Au tip (a = 3.7 μm; R_g = 3.0; $i_{T,\infty}$ = −218.5 nA) in 0.02 M $HClO_4$ – 0.1 M $LiClO_4$ (symbols), and correlations of these curves performed with Eqs. (1)–(3) (solid lines). Dashed lines are the diffusion-controlled dependences.

5. Conclusions

A new theoretical formalism that expands the applicability of SECM for the kinetic analysis of electrode reactions on microelectrode tips was presented in this work. More precisely, the modification of the classical TLC-based SECM theory led to an equation that permits to analyze electron-transfer reactions operating through complex multi-step mechanisms from SECM $I_T(E_T,L)$ curves measured on microelectrode tips. The main requirement is that the reaction mechanism must be solved in a steady-state TLC configuration. As this was previously done for the case of the hydrogen evolution reaction [4], this model was used in this work to analyze the mechanism of this reaction and quantify the kinetic parameters on Pt and Au under mass-transport conditions hardly achievable with other techniques. For the case of Pt, the kinetic parameters are similar to those previously determined. Moreover, what was remarkable in this analysis on Pt is that the transition between mechanistic routes (usually observed in the hydrogen oxidation on microelectrodes [40]) was clearly observed in the hydrogen evolution, which was never reported even when analyzing small microelectrodes [37]. On the other hand, interesting mechanistic aspects of the *her* were also detected on Au. For the first time, it was shown that such transition of routes also occurs on this metal. However, such transition is only observed under high mass-transport rates and at much more negative potentials, since the kinetic parameters for the *her* on Au are very small.

Aknowledgements

This work was supported by Agencia Nacional de Promoción Científica y Tecnológica (ANPCyT), Consejo Nacional de Investigaciones Científicas y Técnicas (CONICET) and Universidad Nacional del Litoral.

References

[1] D.M. Oglesby, S.H. Omang, C.N. Reilley, Anal. Chem. 37 (1965) 1312.
[2] L.B. Anderson, C.N. Reilley, J. Electroanal. Chem. 10 (1965) 295.
[3] A.T. Hubbard, J. Electroanal. Chem. 22 (1969) 165.
[4] J.L. Fernández, J. Electroanal. Chem. 650 (2010) 90.
[5] A.J. Bard, in: A.J. Bard, M.V. Mirkin (Eds.), Scanning Electrochemical Microscopy, Marcel Dekker, New York, 2001, p. 1. Chapter 1.
[6] C. Lefrou, R. Cornut, ChemPhysChem 11 (2010) 547.
[7] A.J. Bard, F.-R. Fan, J. Kwak, O. Lev, Anal. Chem. 61 (1989) 132.
[8] A.J. Bard, G. Denuault, R.A. Friesner, B.C. Dornblaser, L.S. Tuckerman, Anal. Chem. 63 (1991) 1282.
[9] M.V. Mirkin, T.C. Richards, A.J. Bard, J. Phys. Chem. 97 (1993) 7672.
[10] C.G. Zoski, C.R. Luman, J.L. Fernández, A.J. Bard, Anal. Chem. 79 (2007) 4957.
[11] S. Amemiya, N. Nioradze, P. Santhosh, M.J. Deible, Anal. Chem. 83 (2011) 5928.
[12] J. Zhou, Y. Zu, A.J. Bard, J. Electroanal. Chem. 491 (2000) 22.
[13] K. Jambunathan, B.C. Shah, J.L. Hudson, y A.C. Hillier, J. Electroanal. Chem. 500 (2000) 279.
[14] C.G. Zoski, J. Phys. Chem. B 107 (2003) 6401.
[15] S. Jayaraman, A.C. Hillier, J. Phys. Chem. B 107 (2003) 5221.
[16] S. Jarayaman, A.C. Hillier, Langmuir 17 (2001) 7857.
[17] S. Ahmed, S. Li, L. Petrik, V.M. Linkov, Anal. Sci. 20 (2004) 1283.
[18] Y.-C. Weng, C.-T. Hsieh, Electrochim. Acta 56 (2011) 1932.
[19] F.F. Fan, J.L. Fernández, B. Liu, J. Mauzeroll, in: C.G. Zoski (Ed.), Handbook of Electrochemistry, Elsevier, Amsterdam, 2007, p. 511. Chapter 12.
[20] Y. Selzer, I. Turyan, D. Mandler, J. Phys. Chem. B 103 (1999) 1509.
[21] A.R. Kucernak, P.B. Chowdhury, C.P. Wilde, G.H. Kelsall, Y.Y. Zhu, D.E. Williams, Electrochim. Acta 45 (2000) 4483.
[22] F. Li, P. Bertoncello, I. Ciani, G. Mantovani, P.R. Unwin, Adv. Funct. Mater. 18 (2008) 1685.
[23] F. Li, I. Ciani, P. Bertoncello, P.R. Unwin, J. Zhao, C.R. Bradbury, D.J. Fermin, J. Phys. Chem. C 112 (2008) 9686.
[24] E. Gileadi, Electrode Kinetics for Chemists, Chemical Engineers, and Materials Scientists, VCH, New York, 1993, p. 127 (Chapter F).
[25] H.L. Bonazza, J.L. Fernández, J. Electroanal. Chem. 650 (2010) 75.
[26] D.O. Wipf, in: A.J. Bard, M.V. Mirkin (Eds.), Scanning Electrochemical Microscopy, Marcel Dekker, New York, 2001, p. 17. Chapter 2.

[27] M.V. Mirkin, Anal. Chem. 68 (1996) 177a.
[28] W. Miao, Z. Ding, A.J. Bard, J. Phys. Chem. B 106 (2002) 1392.
[29] J.J. Watkins, J. Chen, H.S. White, H.D. Abruña, E. Maisonhaute, C. Amatore, Anal. Chem. 75 (2003) 3962.
[30] P. Sun, M.V. Mirkin, Anal. Chem. 78 (2006) 6526.
[31] X. Lu, Q. Wang, X. Liu, Analytica Chim. Acta 601 (2007) 10.
[32] J. Velmurugan, P. Sun, M.V. Mirkin, J. Phys. Chem. C 113 (2009) 459.
[33] M. Shen, A.J. Bard, J. Am. Chem. Soc. 133 (2011) 15737.
[34] A.M. Bond, K.B. Oldham, C.G. Zoski, J. Electroanal. Chem. 245 (1988) 71.
[35] K.B. Oldham, C.G. Zoski, J. Electroanal. Chem. 256 (1988) 11.
[36] P.M. Quaino, M.R. Gennero de Chialvo, A.C. Chialvo, Electrochim. Acta 52 (2007) 7396.
[37] M.D. Arce, H.L. Bonazza, J.L. Fernández, Electrochim. Acta 107 (2013) 248.
[38] R. Cornut, S. Griveau, C. Lefrou, J. Electroanal. Chem. 650 (2010) 55.
[39] M.R. Gennero de Chialvo, A.C. Chialvo, J. Electroanal. Chem. 415 (1996) 97.
[40] P.M. Quaino, J.L. Fernández, M.R. Gennero de Chialvo, A.C. Chialvo, J. Mol. Catal. A: Chem. 252 (2006) 156.